Electro-Optic Organic Crystal Silicon High-Speed Modulator

D. Korn
M. Jazbinsek
R. Palmer
M. Baier
L. Alloatti
H. Yu
W. Bogaerts
G. Lepage
P. Verheyen
P. Absil
P. Guenter
C. Koos
W. Freude
J. Leuthold
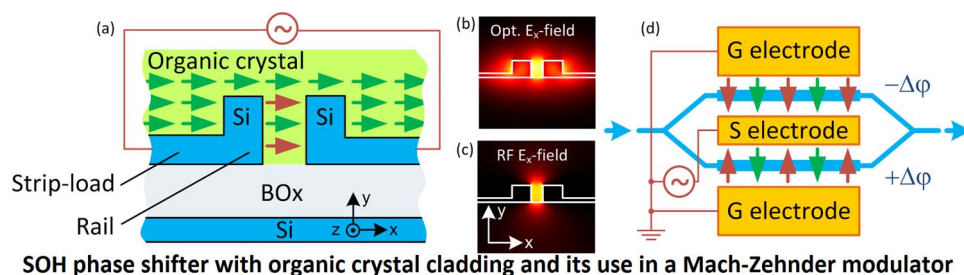
SOH phase shifter with organic crystal cladding and its use in a Mach-Zehnder modulator

Electro-Optic Organic Crystal Silicon High-Speed Modulator

D. Korn,[1] **M. Jazbinsek,**[2] **R. Palmer,**[1] **M. Baier,**[1] **L. Alloatti,**[1] **H. Yu,**[3]
W. Bogaerts,[3] **G. Lepage,**[4] **P. Verheyen,**[4] **P. Absil,**[4] **P. Guenter,**[2]
C. Koos,[1] **W. Freude,**[1] **and J. Leuthold**[1,5]

[1]Institutes IPQ and IMT, Karlsruhe Institute of Technology (KIT), 76131 Karlsruhe, Germany
[2]Rainbow Photonics AG, 8048 Zürich, Switzerland
[3]Department of Information Technology, Photonics Research Group,
Ghent University/IMEC, 9000 Gent, Belgium
[4]IMEC, 3001 Leuven, Belgium
[5] Institute of Electromagnetic Fields, ETH Zurich, Zurich, Switzerland

Abstract: Silicon waveguides can be functionalized with an organic $\chi^{(2)}$-nonlinear cladding. This complements silicon photonics with the electro-optic (EO) effect originating from the cladding and enables functionalities such as pure phase modulation, parametric amplification, or THz-wave generation. Claddings based on a polymer matrix containing chromophores have been introduced, and their strong $\chi^{(2)}$ nonlinearity has already been used to demonstrate ultralow power consuming modulators. However, these silicon–organic hybrid (SOH) devices inherit not only the advantageous properties; these polymer claddings require an alignment procedure called poling and must be operated well below their glass transition temperature. This excludes some applications. In contrast, claddings made from organic crystals come with a different set of properties. In particular, there is no need for poling. This new class of claddings also promises stronger resilience to high temperatures, better long-term stability, and photo-chemical stability. We report on the deposition of an organic crystal cladding of N-benzyl-2-methyl-4-nitroaniline (BNA) on silicon-on-insulator (SOI) waveguides, which have a CMOS-like metal stack on top. Adhering to such an architecture, which preserves the principal advantage of using CMOS-based silicon photonic fabrication processes, permits the first demonstration of high-speed modulation at 12.5 Gbit/s in this material class, which proves the availability of the EO effect from BNA on SOI also for other applications.

Index Terms: Silicon-organic hybrid, silicon-on-insulator, photonic integrated circuit, modulator, organic crystal, electro-optic.

1. Introduction

The telecommunications industry heavily relies on modulators based on the $\chi^{(2)}$ linear electro-optic (EO) effect. Modulators exploiting this effect are popular because they allow for reliable phase and amplitude encoding of the most intricate modulation formats [1] in any desirable pulse shape [2] and

up to highest speed. The general requirements on such modulators are demanding. They should offer lowest drive voltages (V_π) on a small footprint. They should be mass producible, and offer reliable operation under any common environmental condition.

State-of-the art modulators are based on $LiNbO_3$ and meet the above criteria–except that they have a fairly large footprint. They have recently been challenged by integrated GaAs modulators [3] that are more compact. However, industry is interested in silicon photonics as a platform for integrated optics. Making silicon based devices allows resorting to an extensive infrastructure and fabrication experience from the CMOS electronics industry with lithographic resolution for a feature size down to 22 nm. Furthermore, one potentially could fabricate devices more economically. In spite of the many advantages of silicon, this crystalline material does not possess a $\chi^{(2)}$-nonlinearity due to its centro-symmetric structure. There are other options to construct phase modulators with silicon waveguides, e.g., by using the plasma dispersion effect in silicon [4]–[6]. For many applications this presents a simple and effective solution. However, the plasma dispersion effect is inherently related to the plasma absorption effect. Thus, due to the absorption, it can be challenging to precisely access particular points in complex QAM constellation diagrams without pre-distortion of the electrical driving signal.

In addition, new applications based on optical parametric amplification, second harmonic generation for frequency conversion, or mid-IR applications can be implemented using a $\chi^{(2)}$ nonlinearity [7]. The Kerr effect based on a $\chi^{(3)}$-nonlinearity may be used instead of a $\chi^{(2)}$-nonlinearity in some cases. Yet, $\chi^{(3)}$ nonlinearities typically require significantly higher threshold powers [8]. To obtain a $\chi^{(2)}$-nonlinear effect in silicon, strain has been applied, thereby breaking the lattice symmetry [9]–[11]. However, larger nonlinearities can be achieved by employing nonlinear organic materials on the silicon platform. By exploiting the EO effect from chromophores hosted in polymers [12], [13], this so-called silicon-organic hybrid (SOH) approach [14] has already been demonstrated for 40 Gbit/s high-speed phase modulation [15], or 112 Gbit/s IQ modulation using a 16 QAM [16] format. Modulators based on chromophores can excel with very low V_π voltages, resulting in ultra-low power modulators [17]. Unfortunately, the approach with chromophores hosted in polymers has issues on its own. First, operation is limited to be well below the glass transition temperature of the organic material. Second, these devices require an additional fabrication step, in which the chromophore molecules need to be aligned by an external electrical field at each modulator at elevated temperatures. This step is commonly referred to as poling of the nonlinear material and presents an additional effort, especially when producing arrays of modulators in dense photonic integrated circuits (PIC) [18].

The disadvantages due to the use of chromophores hosted in polymers can be overcome by substituting them with a new class of $\chi^{(2)}$-nonlinear materials based on organic crystals. Organic crystals are particularly attractive, as one can choose from a large variety. Organic crystals can be designed to have high melting temperatures and good photo-chemical stability. Therefore, they can withstand harsh conditions. No poling procedure is needed. Some of these crystals are already commercialized for THz-wave generation when irradiated by high-power laser pulses with femtosecond to nanosecond duration [19]. However, special methods have to be developed in order to envelop sub-micrometer silicon waveguide structures with a solid crystal. A low-speed phase shifter made of organic single crystals has been demonstrated [20]. Other successful demonstrations include the testing of a horizontally slotted silicon waveguide filled with such an organic crystal [21], or a tunable organic-crystal micro resonator [22].

In this paper, we demonstrate high-speed EO intensity modulation at 12.5 Gbit/s in a Mach–Zehnder modulator (MZM) employing an organic crystal. We use BNA [23] as a source for the linear electro-optic effect, describe the growth of this organic crystal on silicon waveguides, and quantify the resulting $\chi^{(2)}$-nonlinearity. Fabrication has been done with metal electrode stacks similar to those of standard CMOS electronic circuits in order to maintain CMOS compatibility before the deposition of organic material. Growing an organic crystal on such a silicon photonic chip surface is of particular importance as the CMOS stack permits crossings between optical waveguides and electrical transmission lines. The modulation speed is not limited by the crystal itself, but rather by the electrical transmission line.
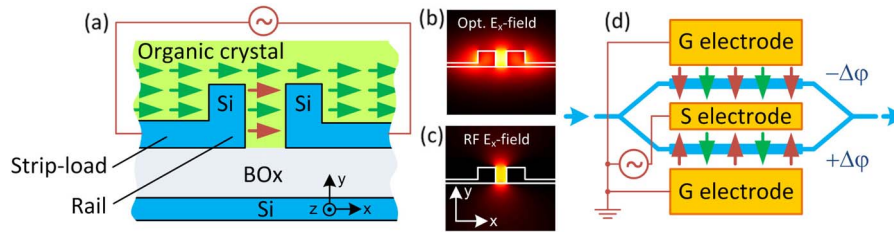
Fig. 1. SOH phase shifter waveguide (WG) with organic crystal cladding and its use in a Mach–Zehnder modulator (MZM). (a) Cross section of strip-loaded slot WG to be used with light in quasi-TE mode. Strongest diagonal $\chi^{(2)}$-tensor element of organic crystal cladding (polar axis indicated by green arrows) in the direction of the applied RF field (red arrows). (b) Cross section of color-coded dominant x-component $|E_x|$ of the optical E-field in quasi-TE mode in the strip-loaded slot WG. (c) Electrical RF field in x-direction (red arrows in subfigures). (d) Mach–Zehnder interferometer modulator (MZM) with optical waveguides in blue, electrical connections in red, ground-signal-ground electrodes (GSG) of coplanar transmission line in yellow. In each arm of the interferometer a phase modulator section is inserted. It consists of a strip-loaded slot WG. Note that the organic crystal has the same orientation in both arms, such that an electrical field applied to the central signal electrode (S) will introduce opposite phase shifts. This mode of operation is called "push-pull" and allows pure amplitude or intensity modulation without any phase modulation.

2. Silicon-Organic Hybrid (SOH) Concept Employing Organic Crystals

The structure of an SOH phase-shifter and the MZI configuration used to achieve intensity modulation is depicted in Fig. 1. An organic cladding material is placed to cover an optical waveguide such that the organic material interacts with the optical field of the SOI waveguide (WG). A particular strong overlap [24] of the guided light with the organic cladding is obtained with the so-called strip-loaded slot WG structure shown in Fig. 1(a). In this structure the optical field is enhanced in the slot as the refractive index is lower in the slot than in the silicon rails, see Fig. 1(b). The confinement of light to the organic material is best for a quasi-TE mode, where the dominant electric field component is in x-direction, i.e., parallel to the substrate plane, Fig. 1(b). To induce a phase-shift by means of the $\chi^{(2)}$-nonlinear effect, an RF voltage must be applied across the slot, Fig. 1(c), for controlling the refractive index of the cladding. Switching is fast, if the strip-loads and rails are sufficiently doped in order to guarantee a good conductivity and therefore allow a fast charging and discharging of the slot capacitance. However, excessive doping leads to excessive optical losses. The two silicon rails are electrically connected by the silicon strip-loads to metal electrodes far away from the optical field in the slot, Fig. 1(d). The $\chi^{(2)}$-nonlinear refractive index change is most efficient, if the largest organic cladding's diagonal $\chi^{(2)}$-tensor element [green arrows in Fig. 1(a)] is aligned along the x-axis perpendicularly to the slot sidewalls and thereby in the direction of the modulating RF field $E_{x,\mathrm{RF}}$ (red arrows). In a bulk material with EO coefficient r and a plane wave (wavelength λ) one then can expect a phase shift in the order $\Delta\varphi = \Gamma(\pi/\lambda)Ln^3r\,E_{x,\mathrm{RF}}$ for a device of length L in a homogeneous material with refractive index n and a confinement Γ of the optical mode in the slot. The product n^3r is used as an EO figure of merit (FOM) to describe the ability of an EO material to shift the phase of an optical wave upon application of a modulating voltage.

For intensity modulation the phase-shifters are typically arranged in the two arms of an MZI, Fig. 1(d). The phase shift in each arm is controlled by the ground-signal-ground electrodes of a coplanar transmission line [25], [26]. Since the electro-optic material is arranged along one direction only, the optical fields in the two arms experience phase shifts in opposite direction when they are operated with the GSG electrodes. This is called push-pull operation mode of the MZM.

To apply an organic EO cladding we have two choices:

- One may apply polymers which host chromophores [15], [27]. This is frequently done because of the large electro-optic coefficient r and resulting large FOM. However, the chromophores need a one-time alignment ("poling") in order to develop a macroscopic EO effect. Also, there might be an issue when using the polymers at elevated temperatures, because the chromophores might slowly lose alignment even before the polymer's glass transition temperature is reached.
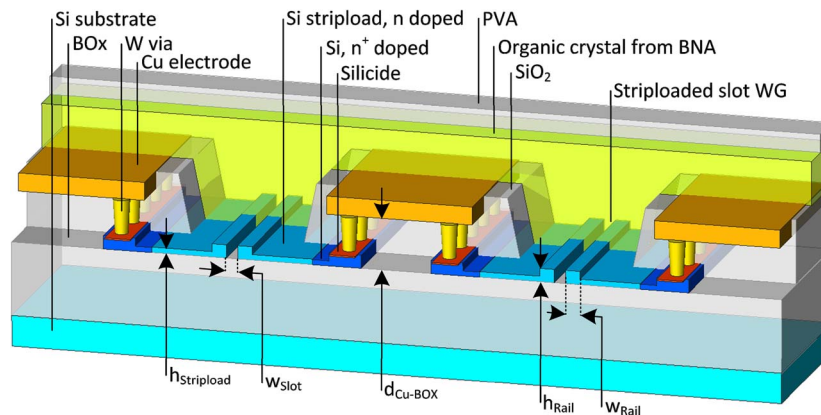
Fig. 2. Cross section of MZM employing an organic crystal (not drawn to scale). Two phase modulator sections are displayed consisting of strip-loaded slot WGs, which are filled with a nonlinear organic BNA cladding. The silicon rails are connected to ground-signal-ground electrodes of a coplanar transmission line through the Si strip-loads, a silicide layer and tungsten vias. This electrode arrangement allows crossings of optical WGs and electrical transmission lines. This architecture corresponds to the metal stack technology well known from the CMOS platform.

- In contrast, the material class comprising organic EO crystals offers the advantage that the chromophores composing these crystals keep their alignment as determined by the crystal structure up to the crystal melting temperature (provided the molecules remain chemically stable). Hence, using materials from the class of organic crystals promises long-term stability even at elevated temperatures and high illumination intensities due to their superior photo-chemical stability [28].

An overview of available materials of this class is given in [29], p. 163. in [30]. A few examples are listed here for reference: Stilbazolium salt crystals like DAST (4-N, N-dimethylamino-4'-N'-methyl-stilbazolium tosylate) with $n^3 r = 480$ pm/V melting at 256 °C [31], DAPSH (trans-4-dimethylamino-N-phenyl-stilbazolium hexafluorophosphate) with $n^3 r > 500$ pm/V, and DSTMS (4-N, N-dimethylamino-4'-N'-methyl-stilbazolium 2,4,6-trimethylbenzenesulfonate) with $n^3 r = 480$ pm/V melting at 258 °C [32]. However, DAST, DAPSH, and DSTMS are not stable at melting temperatures, so only solution growth is possible [29]. Furthermore, configurationally locked polyene molecular crystals have been developed [7], which are stable upon melting, which makes melt growth possible. These materials deliver similarly high effective nonlinearities. Examples are OH1 (2-(3-(4-hydroxystyryl)-5, 5-dimethylcyclohex-2-enylidene)malononitrile) $n^3 r = 470$ pm/V melting at 212 °C, or OH2 with an expected FOM of $n^3 r > 600$ pm/V melting at 242 °C.

Here, we use an organic crystal made from BNA [23]. It has a high diagonal nonlinear optical coefficient $d_{333} = 234$ pm/V at 1064 nm [23] and a relatively low melting temperature of 105 °C. Nevertheless, we chose BNA for our proof-of-principle experiments, because it was easy to grow due to the low melting point and its reasonable wetting properties on a CMOS-structured silicon chip.

3. SOH Device Fabrication and Experiments

Mach–Zehnder modulators with SOH waveguides comprising the organic BNA crystal as a cladding and standard CMOS metal stack electrodes have been fabricated. After structuring the SOI wafer, we cover the SOI WGs with a thin film of the organic crystal BNA and open areas for electrical contacting to supply the modulating voltage. To verify and quantify the resulting EO effect, we use the modulator to encode data on an optical carrier.

3.1. Fabrication of an SOH Modulator

In Fig. 2 the cross section of an MZM consisting of two strip-loaded slot WGs is shown, in our implementation with a CMOS-like metal stack. The organic crystal BNA fills the WG slots. Other

chips from the same wafer have been used before to make EO modulators based on EO-active chromophores hosted in a polymer [16].

The fabrication of the passive part follows Ref. [16]: SOI wafers (SOITEC) with a WG layer (220 nm high) on a buried oxide (Box, 2 μm thick) are processed employing 193 nm deep UV lithography at IMEC. Slot WGs ($w_{\text{Slot}} = 125$ nm, $w_{\text{Rail}} = 220$ nm, $h_{\text{Rail}} = 220$ nm) with attached n-doped silicon striploads ($h_{\text{Stripload}} = 50$ nm, arsenic doping with a nominal concentration of 3×10^{17} cm^{-3}) are etched into the WG layer. Standard strip and rib WGs for low-loss access waveguides [33] and standard grating couplers [34] are structured by dry etching 70 nm of Si.

The copper electrodes (coplanar RF transmission lines guiding the electrical modulating wave) and the strip-loaded slot WG (guiding the light) are connected by conducting tungsten-filled (W) vias and a silicide film (surrounded by highly doped silicon with a concentration of nominally 1×10^{20} cm^{-3}). Dielectric layers of mostly SiO$_2$ and Si$_3$N$_4$ support the Cu electrodes and fix the distance between Cu electrode and BOx to $d_{\text{Cu−BOx}} = 1.1$ μm. This metal stack could be extended with additional standard layers, e.g., making aluminum pads for packaging. However, in our case we end the stack with a thin layer of SiC to protect Cu from air. The slot WGs are 1.5 mm long and terminated at each end with a transition from the slot WG to standard strip WGs using low-loss converters [35]. Multi-mode interference (MMI) couplers split the input field and combine the fields in the two interferometer arms.

The trenches to expose the slots are opened by dry and wet etching of the dielectric layers, which are then filled with BNA that in turn is covered with a layer of polyvinyl alcohol (PVA).

3.2. Deposition of Organic Crystal BNA

In integrated optics, there are various possibilities to fabricate claddings of organic single-crystal structures [29], [36]. In the past, bulk crystals of DAST have been grown and placed on top of silicon waveguides [31]. For this an elaborated polishing procedure is required, and obtaining a good optical contact between a crystal and an SOI chip surface is a challenge. Moreover, the thickness of the crystal might be inconvenient when attempting to contact modulation electrodes. Another method relies on growing single-crystalline thin films of various crystals such as DAST and DSTMS from a solution between glass plates. However, transferring the thin films to the chip implies the risk of fractures. Thus, for processing a full wafer, on-chip crystal growth seems to be the only viable option. For chips with very smooth topography, single-crystalline films of OH1 have been successfully grown directly from solutions on SOI chips [29], which takes several weeks. The most versatile technique, however, is to fabricate organic single-crystalline films by using melt growth. Using this approach, thin organic single-crystalline wires with a thickness down to 25 nm have already been grown on glass [37], and also more complex waveguiding structures such as microring resonators were fabricated [22].

Here, we opt for direct, on-chip growth of BNA from the melt. This approach is not impeded by the rugged surface (due to the CMOS metal stack), shows reasonably large growth rates (hours), and provides a high-purity crystal. The crystalline symmetry of BNA is orthorhombic *mm*2. Its melting temperature is relatively low, about 105 °C, which is the limiting temperature for post-processing possibilities. BNA thin films always grow along the *ac* crystallographic plane with the fastest growth along the *a* direction, i.e., normal to the polar axis *c* [21], which we confirmed by polarized second-harmonic generation experiments. Therefore, when we manage to induce the growth of BNA crystals along the WG direction, its largest $\chi^{(2)}$-tensor element $\chi^{(2)}_{333}$ coincides with the E_x-field of the quasi-TE mode in the slot WGs.

We employ the following procedure to grow BNA films: **(1)** Place a flat glass plate (a 200 μm thick borosilicate glass wafer) covering the target area on the Si chip. Deposit the BNA as powder on one side perpendicularly to the phase modulator sections of the WGs as shown in Fig. 3(a). **(2)** In vacuum, heat the whole sample up to 120 °C, well above the melting temperature of BNA to decrease the viscosity of liquid BNA. The capillary effect between SOI chip and glass plate pulls the liquid BNA below the glass plate, see Fig. 3(b). The wetting properties for BNA on both SOI and glass are sufficient to obtain a nice capillary flow. In case of other materials special surface treatment might be necessary. The vacuum helps to prevent voids when filling. **(3)** After a few minutes, the melt is
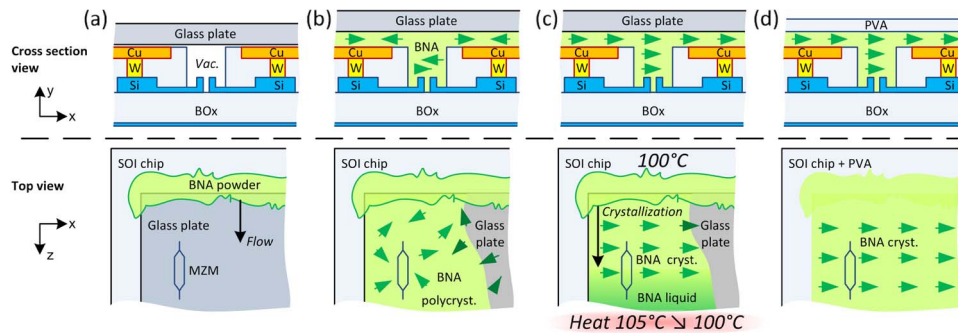
Fig. 3. Deposition method for growth of an organic single crystal thin film on top of strip-loaded slot WGs. **Upper row:** Cross-section of one phase modulator section as in Fig. 2. Subfigures (a) ... (d) show various stages of the deposition process. BNA (green shading) covers the chip and fills the slot beneath an auxiliary glass plate (grey shading). **Lower row:** Top view of chip (light grey shading) with auxiliary glass plate on top (grey shading). BNA (green shading) fills the space above the chip and below the auxiliary glass plate. The deposition starts by putting BNA powder at one edge of the auxiliary glass plate. More precisely: (a) A vacuum is maintained between glass plate and chip. (b) Applying heat melts the BNA powder, which is drawn into the gap between glass plate and chip due to the capillary effect. Polycrystalline BNA forms after a fast cool-down process. No macroscopic $\chi^{(2)}$-nonlinearity is to be seen. Green arrows indicate the random orientation of the polar axis of the polycrystalline domains. (c) Region of applied BNA power is heated to a fixed temperature of 100 °C close to but below the melting point ("cold" side). An additional local heat source increases the temperature of the opposite ("hot") side to a temperature of 105 °C, which is above the melting point. When removing the additional local heat source, the temperature of the hot side is reducing back to 100 °C. Beginning with a random orientation at the cold side, a single crystal then grows along the fastest growth direction which is oriented towards the formerly hot side. (d) After removal of the auxiliary glass plate, a PVA cover is spin-coated to fill any cracks in the BNA for reducing scattering in the WGs.

distributed homogeneously below the glass plate. Then the vacuum is replaced by nitrogen at normal atmospheric pressure, and the sample is quickly cooled down to room temperature. This leads to fast crystallization of BNA. However, the resulting film is polycrystalline due to its fast growth well below the melting temperature. **(4)** To get the same single-crystal orientation in all the phase modulator sections, a controlled crystallization is necessary. By heating the entire chip covered with polycrystalline BNA to just below the melting temperature (100 °C) and by keeping one side at a fixed temperature above the melting point (105 °C), the polycrystal melts again, but only at the "hot" side. **(5)** When removing the additional, one-sided heat source, the temperature of the "hot" side reduces back to 100 °C. Starting with a random orientation at the "cold" side, the crystal then grows along its fastest growth direction, which is oriented towards the formerly "hot" side, Fig. 3(c). Note that spontaneous nucleation of BNA does not occur at this temperature unless cooled down well below the melt temperature, as done in step (3). Hence, it is assured that the film only starts growing from the "cold" top (seed) area. **(6)** To access the RF electrodes the glass plate is removed as shown in Fig. 3(d), and the entire chip is spin-coated with polyvinyl alcohol (PVA) to reduce scattering from potential crystal fractures induced by removal of the glass plate.

The direction of the optical axis of the BNA crystal was determined with a reflection microscope by placing and rotating the sample between crossed polarizers, thereby measuring the crystal's birefringence. In different deposition attempts we achieved a crystalline orientation deviating from the optimal direction of the polar axis by $\alpha = 10° \ldots 40°$. Additional growth-guiding trenches on chip or in the auxiliary glass plate could optimize the orientation further (for well-defined micro-sized channels the growth direction aligns perfectly [21], [22], [37]). We manually removed the organic crystal locally for contacting the electrodes with RF probes. In practice, lithographic processes [20] for structuring organic crystals will be preferred.

3.3. SOH Modulator for Data Generation

The viability of the EO modulation concept and successful deposition of BNA is demonstrated in an experiment. Fig. 4(a) depicts the setup. A 12.5 Gbit/s electrical data signal with a non-return-to-zero
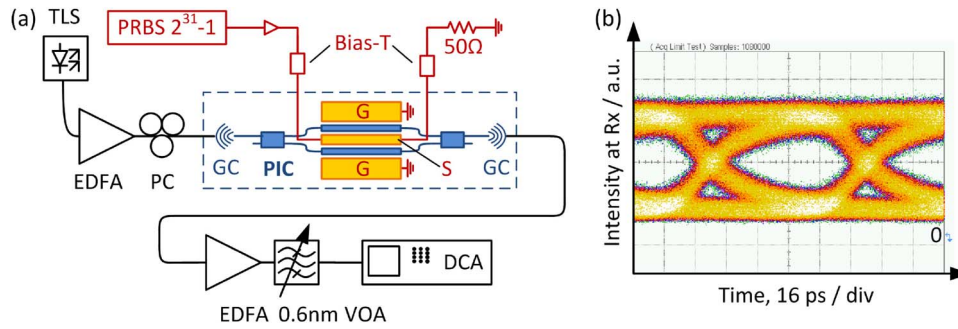
Fig. 4. Experimental setup for demonstrating the EO effect of a hybridly integrated organic crystal. Optical on-chip connections are in blue, electrical connections are drawn in red. (a) CW light from a tunable laser source (TLS) is amplified by an erbium-doped fiber amplifier (EDFA), polarization-controlled (PC), and coupled by a grating coupler (GC) to one input of a multimode interference (MMI) coupler. The MMI maps the light onto the two arms of the Mach–Zehnder interferometer modulator with phase modulators in its arms as discussed in Fig. 2. Another MMI recombines the fields. This light is coupled back to a fiber by means of a GC and guided to the receiver. The receiver consists of an EDFA, a filter and a digital communication analyzer (DCA). A pseudo-random binary sequence (PRBS) is amplified, and passed through a bias-T for adjusting the MZM to the quadrature operating point. Ground-signal-ground (GSG) electrodes excite an electrical traveling wave, which modulates the incoming light, which is evaluated in the receiver. (b) Eye diagram of the received optical signal at 12.5 Gbit/s. A quality factor Q^2 corresponding to 14 dB evaluates to a bit error ratio (BER) of 3×10^{-7}.

pseudo-random binary sequence (PRBS) of length $2^{31} - 1$ is generated and amplified to nominally $V_{pp} = 8$ V. RF probes bring this signal to the SOH MZM and terminate the electrodes with an off-chip resistor of 50 Ω. Two bias-Ts allow adding a DC voltage for adjusting the MZM to its quadrature operating point for intensity modulation. Light with a wavelength of 1538 nm from a tunable laser source (TLS) is amplified in an erbium-doped fiber amplifier (EDFA) to a power of 18 dBm, and coupled via a grating coupler (GC) to the MZM. The resulting on-off keyed (OOK) optical signal is collected at the output GC, amplified, filtered, and received with a digital communication analyzer (DCA).

In this first generation chip we measured relatively high fiber-to-fiber losses. Potential loss sources have been identified. They are as follows: 1) Coupling losses of about 5 dB for each GC. In a commercial implementation more effort would be made to improve this loss. More elaborate GCs exhibit losses of 1.6 dB per coupler [38]. Inverted tapers for butt coupling of external fibers were demonstrated to have a loss of 0.7 dB [39]. 2) Losses of about 5 dB/cm in the 7 mm long access WGs, which have bends and strip-to-ridge waveguide transitions. Further we have losses of about 1.5 dB in strip waveguides by scattering due to WG sidewall roughness and by absorption due to the crossing metal electrodes. 3) Excess loss of about 1 dB for each of the two MMIs adds to the splitting loss of 3 dB. 4) Loss of about 1 dB in each of the two strip-to-slot transitions. 5) Loss in the phase modulator section of about 16 dB. A reduction of losses seems to be relatively straight-forward for all issues observed in 1)–4), so that device insertion loss effectively is only limited by the loss in the phase modulator section. The slot WG sidewall roughness could be improved by using atomic layer deposition [40], which at the same time could enhance the wetting properties for organic crystal growth.

Further, variations in the fabrication process have led to an imbalance of the loss in both arms of the MZM. An extinction ratio of more than 6 dB was measured with modulation, as can be seen from the eye diagram Fig. 4(b). The 3 dB-bandwidth of the MZM was measured to be about 7 GHz. It is limited by the RC constant of the structure and RF wave propagation losses [16]. The V_π-voltage at DC is around 8 V leading to a $V_\pi L$ product of 12 Vmm. This corresponds to a figure of merit (FOM) for the EO coefficient of $n^3 r = 31$ pm/V. Evaluation of the open eye diagram in Fig. 4(b) of the received optical signal indicates a signal quality Q^2 of 14 dB, which translates into a bit error ratio (BER) of 3×10^{-7}. From the nonlinear coefficients d_{333}, d_{311} and refractive indices reported in [22] and using the same model as in [28] we estimate the EO coefficients of the organic crystal BNA to be $r_{33} = 24$ pm/V and $r_{13} \sim r_{51}$ to be negligible. The expected material's FOM should be in the order of

$n_3^3 r_{33} = 135$ pm/V. Taking the measured crystal misalignment of $\alpha = 34°$ of the device under test into account, we would expect a FOM of $n_\alpha^3 r_{33} \cos^3 \alpha = 67$ pm/V. However, with a value of 31 pm/V we only find a value that is about half of the expected nonlinearity. As a reason for this discrepancy, we suspect either imperfect filling of the slot WG (as the wet-etch step might have partly under-etched the WG and thus might have produced voids with imperfect crystal growth), or an overestimation of the original material's EO coefficient.

4. Conclusion

We demonstrated data modulation at 12.5 Gbit/s using an organic crystal of BNA integrated on SOI strip-loaded slot waveguides in a Mach–Zehnder modulator configuration. We showed that an important class of claddings, namely organic EO crystals, is compatible with the CMOS-typical metal stack used for traveling wave electrodes. Compared to frequently investigated, polymer-based EO claddings, our technique represents a viable alternative for fabricating high-speed modulators for advanced modulation formats. Organic EO crystal claddings pave the way for silicon-organic hybrid modulators with higher operating temperatures and better overall stability. This allows running the devices at larger optical input powers. Due to the strong light confinement, exceptionally large intensities can easily be reached, which might turn out to be useful not only for modulators but also for efficient THz-wave generation and for parametric amplification.

References

[1] Y. Koizumi, K. Toyoda, M. Yoshida, and M. Nakazawa, "1024 QAM (60 Gbit/s) single-carrier coherent optical transmission over 150 km," *Opt. Exp.*, vol. 20, no. 11, pp. 12508–12514, May 2012.

[2] J. Leuthold and W. Freude, "Chapter 9—Optical OFDM and Nyquist Multiplexing," in *Optical Fiber Telecommunications*, I. P. Kaminow, T. Li, and A. E. Willner, Eds., 6th ed. Boston, MA, USA: Academic, 2013, pp. 381–432.

[3] D. Korn, P. C. Schindler, C. Stamatiadis, M. F. O'Keefe, L. Stampoulidis, R. M. Schmogrow, P. Zakynthinos, R. Palmer, N. Cameron, Y. Zhou, R. G. Walker, E. Kehayas, I. Tomkos, L. Zimmermann, K. Petermann, W. Freude, C. Koos, and J. Leuthold, "First monolithic GaAs IQ electro-optic modulator, demonstrated at 150 Gbit/s with 64-QAM," presented at the Optical Fiber Communication Conference/National Fiber Optic Engineers Conference, Anaheim, CA, USA, 2013, Paper PDP5C.4.

[4] W. M. Green, M. J. Rooks, L. Sekaric, and Y. A. Vlasov, "Ultra-compact, low RF power, 10 Gb/s silicon Mach–Zehnder modulator," *Opt. Exp.*, vol. 15, no. 25, pp. 17 106–17 113, Dec. 2007.

[5] L. Liao, A. Liu, D. Rubin, J. Basak, Y. Chetrit, H. Nguyen, R. Cohen, N. Izhaky, and M. Paniccia, "40 Gbit/s silicon optical modulator for high-speed applications," *Electron. Lett.*, vol. 43, no. 22, pp. 1196–1197, Oct. 2007.

[6] D. J. Thomson, F. Y. Gardes, J.-M. Fedeli, S. Zlatanovic, Y. Hu, B. P. P. Kuo, E. Myslivets, N. Alic, S. Radic, G. Z. Mashanovich, and G. T. Reed, "50-Gb/s silicon optical modulator," *IEEE Photon. Technol. Lett.*, vol. 24, no. 4, pp. 234–236, Feb. 2012.

[7] O.-P. Kwon, S.-J. Kwon, M. Jazbinsek, F. D. J. Brunner, J.-I. Seo, C. Hunziker, A. Schneider, H. Yun, Y.-S. Lee, and P. Günter, "Organic phenolic configurationally locked polyene single crystals for electro-optic and terahertz wave applications," *Adv. Funct. Mater.*, vol. 18, no. 20, pp. 3242–3250, Oct. 2008.

[8] L. Alloatti, D. Korn, C. Weimann, C. Koos, W. Freude, and J. Leuthold, "Second-order nonlinear silicon-organic hybrid waveguides," *Opt. Exp.*, vol. 20, no. 18, pp. 20 506–20 515, Aug. 2012.

[9] R. S. Jacobsen, K. N. Andersen, P. I. Borel, J. Fage-Pedersen, L. H. Frandsen, O. Hansen, M. Kristensen, A. V. Lavrinenko, G. Moulin, H. Ou, C. Peucheret, B. Zsigri, and A. Bjarklev, "Strained silicon as a new electro-optic material," *Nature*, vol. 441, no. 7090, pp. 199–202, May 2006.

[10] B. Chmielak, M. Waldow, C. Matheisen, C. Ripperda, J. Bolten, T. Wahlbrink, M. Nagel, F. Merget, and H. Kurz, "Pockels effect based fully integrated, strained silicon electro-optic modulator," *Opt. Exp.*, vol. 19, no. 18, pp. 17212–17219, Aug. 2011.

[11] C. Matheisen, M. Nagel, S. Sawallich, M. Waldow, B. Chmielak, T. Wahlbrink, J. Bolten, and H. Kurz, "Locally induced electro-optic activity in silicon nanophotonic devices," presented at the CLEO/EUROPE—IQEC, Munich, Germany, 2013.

[12] J.-M. Brosi, C. Koos, L. C. Andreani, M. Waldow, J. Leuthold, and W. Freude, "High-speed low-voltage electro-optic modulator with a polymer-infiltrated silicon photonic crystal waveguide," *Opt. Exp.*, vol. 16, no. 6, pp. 4177–4191, Mar. 2008.

[13] J. H. Wülbern, A. Petrov, and M. Eich, "Electro-optical modulator in a polymerinfiltrated silicon slotted photonic crystal waveguide heterostructure resonator," *Opt. Exp.*, vol. 17, no. 1, pp. 304–313, Jan. 2009.

[14] J. Leuthold, W. Freude, J.-M. Brosi, R. Baets, P. Dumon, I. Biaggio, M. L. Scimeca, F. Diederich, B. Frank, and C. Koos, "Silicon organic hybrid technology—A platform for practical nonlinear optics," *Proc. IEEE*, vol. 97, no. 7, pp. 1304–1316, Jul. 2009.

[15] L. Alloatti, D. Korn, R. Palmer, D. Hillerkuss, J. Li, A. Barklund, R. Dinu, J. Wieland, M. Fournier, J. Fedeli, H. Yu, W. Bogaerts, P. Dumon, R. Baets, C. Koos, W. Freude, and J. Leuthold, "42.7 Gbit/s electro-optic modulator in silicon technology," *Opt. Exp.*, vol. 19, no. 12, pp. 11841–11851, Jun. 2011.

[16] D. Korn, R. Palmer, H. Yu, P. C. Schindler, L. Alloatti, M. Baier, R. Schmogrow, W. Bogaerts, S. K. Selvaraja, G. Lepage, M. Pantouvaki, J. M. D. Wouters, P. Verheyen, J. Van Campenhout, B. Chen, R. Baets, P. Absil, R. Dinu, C. Koos, W. Freude, and J. Leuthold, "Silicon-Organic Hybrid (SOH) IQ modulator using the linear electro-optic effect for transmitting 16QAM at 112 Gbit/s," *Opt. Exp.*, vol. 21, no. 11, pp. 13 219–13 227, Jun. 2013.

[17] R. Palmer, L. Alloatti, D. Korn, P. C. Schindler, M. Baier, J. Bolten, T. Wahlbrink, M. Waldow, R. Dinu, W. Freude, C. Koos, and J. Leuthold, "Low power Mach–Zehnder modulator in silicon-organic hybrid technology," *IEEE Photon. Technol. Lett.*, vol. 25, no. 13, pp. 1226–1229, Jul. 2013.

[18] H. Chen, B. Chen, D. Huang, D. Jin, J. D. Luo, A. K.-Y. Jen, and R. Dinu, "Broadband electro-optic polymer modulators with high electro-optic activity and low poling induced optical loss," *Appl. Phys. Lett.*, vol. 93, no. 4, pp. 043507-1–043507-3, Jul. 2008.

[19] Rainbow Photonics AG, Zürich, Switzerland, 2013. [Online]. Available: http://www.rainbowphotonics.com/

[20] C. Hunziker, S.-J. Kwon, H. Figi, M. Jazbinsek, and P. Günter, "Fabrication and phase modulation in organic single-crystalline configurationally locked, phenolic polyene OH1 waveguides," *Opt. Exp.*, vol. 16, no. 20, pp. 15 903–15 914, Sep. 2008.

[21] H. Figi, D. H. Bale, A. Szep, L. R. Dalton, and A. Chen, "Electro-optic modulation in horizontally slotted silicon/organic crystal hybrid devices," *J. Opt. Soc. Amer. B, Opt. Phys.*, vol. 28, no. 9, pp. 2291–2300, Sep. 2011.

[22] H. Figi, M. Jazbinsek, C. Hunziker, M. Koechlin, and P. Günter, "Electro-optic tuning and modulation of single-crystalline organic microring resonators," *J. Opt. Soc. Amer. B, Opt. Phys.*, vol. 26, no. 5, pp. 1103–1110, May 2009.

[23] M. Fujiwara, M. Maruyama, M. Sugisaki, H. Takahashi, S. Aoshima, R. J. Cogdell, and H. Hashimoto, "Determination of the d-tensor components of a single crystal of N-benzyl-2-methyl-4-nitroaniline," *Jpn. J. Appl. Phys.*, vol. 46, no. 4A, pp. 1528–1530, Apr. 2007.

[24] J. Leuthold, C. Koos, W. Freude, L. Alloatti, R. Palmer, D. Korn, J. Pfeifle, M. Lauermann, R. Dinu, S. Wehrli, M. Jazbinsek, P. Gunter, M. Waldow, T. Wahlbrink, J. Bolten, H. Kurz, M. Fournier, J.-M. Fedeli, H. Yu, and W. Bogaerts, "Silicon-organic hybrid electro-optical devices," *IEEE J. Sel. Topics Quantum Electron.*, vol. 19, no. 6, p. 3401413, Nov./Dec. 2013.

[25] J. Witzens, T. Baehr-Jones, and M. Hochberg, "Design of transmission line driven slot waveguide Mach–Zehnder interferometers and application to analog optical links," *Opt. Exp.*, vol. 18, no. 16, pp. 16 902–16 928, Aug. 2010.

[26] R. Ding, T. Baehr-Jones, Y. Liu, R. Bojko, J. Witzens, S. Huang, J. Luo, S. Benight, P. Sullivan, J.-M. Fedeli, M. Fournier, L. Dalton, A. Jen, and M. Hochberg, "Demonstration of a low $V_{\pi}L$ modulator with GHz bandwidth based on electro-optic polymer-clad silicon slot waveguides," *Opt. Exp.*, vol. 18, no. 15, pp. 15 618–15 623, Jul. 2010.

[27] R. Palmer, L. Alloatti, D. Korn, P. C. Schindler, R. Schmogrow, W. Heni, S. Koenig, J. Bolten, T. Wahlbrink, M. Waldow, H. Yu, W. Bogaerts, P. Verheyen, G. Lepage, M. Pantouvaki, J. Van Campenhout, P. Absil, R. Dinu, W. Freude, C. Koos, and J. Leuthold, "Silicon-organic hybrid MZI modulator generating OOK, BPSK and 8-ASK signals for up to 84 Gbit/s," *IEEE Photon. J.*, vol. 5, no. 2, p. 6600907, Apr. 2013.

[28] D. Rezzonico, S.-J. Kwon, H. Figi, O.-P. Kwon, M. Jazbinsek, and P. Günter, "Photochemical stability of nonlinear optical chromophores in polymeric and crystalline materials," *J. Chem. Phys.*, vol. 128, no. 12, p. 124 713, Mar. 2008.

[29] M. Jazbinsek, H. Figi, C. Hunziker, B. Ruiz, S.-J. Kwon, O.-P. Kwon, Z. Yang, and P. Günter, "Organic electro-optic single crystalline films for integrated optics," in *Proc. Linear Nonlinear Opt. Organic Mater. X*, San Diego, CA, USA, 2010, pp. 77740Q-1–77740Q-10.

[30] P. Günter, *Nonlinear Optical Effects and Materials*. Berlin, Germany: Springer-Verlag, 2000.

[31] M. Jazbinsek, L. Mutter, and P. Gunter, "Photonic applications with the organic nonlinear optical crystal DAST," *IEEE J. Sel. Topics Quantum Electron.*, vol. 14, no. 5, pp. 1298–1311, Sep./Oct. 2008.

[32] L. Mutter, F. D. Brunner, Z. Yang, M. Jazbinsek, and P. Günter, "Linear and nonlinear optical properties of the organic crystal DSTMS," *J. Opt. Soc. Amer. B, Opt. Phys.*, vol. 24, no. 9, pp. 2556–2561, Sep. 2007.

[33] W. Bogaerts and S. K. Selvaraja, "Compact single-mode silicon hybrid rib/strip waveguide with adiabatic bends," *IEEE Photon. J.*, vol. 3, no. 3, pp. 422–432, Jun. 2011.

[34] F. van Laere, T. Claes, J. Schrauwen, S. Scheerlinck, W. Bogaerts, D. Taillaert, L. O'Faolain, D. Van Thourhout, and R. Baets, "Compact focusing grating couplers for silicon-on-insulator integrated circuits," *IEEE Photon. Technol. Lett.*, vol. 19, no. 23, pp. 1919–1921, Dec. 2007.

[35] R. Palmer, L. Alloatti, D. Korn, W. Heni, P. C. Schindler, J. Bolten, M. Karl, M. Waldow, T. Wahlbrink, W. Freude, C. Koos, and J. Leuthold, "Low-loss silicon strip-to-slot mode converters," *IEEE Photon. J.*, vol. 5, no. 1, p. 2200409, Feb. 2013.

[36] M. Jazbinsek and P. Gunter, "Organic electrooptic crystal modulators," in *Broadband Optical Modulators: Science, Technology, and Applications*, A. Chen and E. J. Murphy, Eds. Boca Raton, FL, USA: CRC Press, 2011.

[37] H. Figi, M. Jazbinsek, C. Hunziker, M. Koechlin, and P. Günter, "Electro-optic single-crystalline organic waveguides and nanowires grown from the melt," *Opt. Exp.*, vol. 16, no. 15, pp. 11 310–11 327, Jul. 2008.

[38] D. Vermeulen, S. Selvaraja, P. Verheyen, G. Lepage, W. Bogaerts, P. Absil, D. Van Thourhout, and G. Roelkens, "High-efficiency fiber-to-chip grating couplers realized using an advanced CMOS-compatible silicon-on-insulator platform," *Opt. Exp.*, vol. 18, no. 17, pp. 18 278–18 283, Aug. 2010.

[39] M. Pu, L. Liu, H. Ou, K. Yvind, and J. M. Hvam, "Ultra-low-loss inverted taper coupler for silicon-on-insulator ridge waveguide," *Opt. Commun.*, vol. 283, no. 19, pp. 3678–3682, Oct. 2010.

[40] T. Alasaarela, D. Korn, L. Alloatti, A. Säynätjoki, A. Tervonen, R. Palmer, J. Leuthold, W. Freude, and S. Honkanen, "Reduced propagation loss in silicon strip and slot waveguides coated by atomic layer deposition," *Opt. Exp.*, vol. 19, no. 12, pp. 11 529–11 538, Jun. 2011.